

# Kinetic Modeling of Langmuir Probe Characteristics in a Laboratory Plasma near a Conducting Body

Saeed ur Rehman,<sup>1, a)</sup> Lisa E. Fisher,<sup>2</sup> Kristina A. Lynch,<sup>2</sup> and Richard Marchand<sup>3</sup>

<sup>1)</sup>*Theoretical Physics Division, PINSTECH, Nilore Islamabad 44000, Pakistan*

<sup>2)</sup>*Department of Physics and Astronomy, Dartmouth College, Hanover, New Hampshire 03755, USA*

<sup>3)</sup>*Department of Physics, University of Alberta, Edmonton AB, T6G 2E1, Canada*

Results are presented from kinetic modeling of Langmuir probe characteristics measured in the vicinity of a conducting sphere, in a well controlled laboratory plasma. In the experiment, the interaction of a drifting argon plasma with a conducting spherical sphere is studied using two cylindrical Langmuir probes located upstream and downstream of the sphere. Plasma parameters upstream of the sphere are determined by fitting an experimentally measured characteristic with the one obtained from simulations. Using the same upstream plasma parameters as input in simulations, the characteristic computed in the wake of the sphere is compared with the measured one. In addition to validating our simulation model for this type of experiment, the comparison serves to illustrate the importance of effects often neglected in the interpretation of Langmuir probe measurements, such as plasma with gradients and Earth magnetic field.

## I. INTRODUCTION

The Experimental Low Energy Plasma for Hemispherical Analyzer Nominal Testing (ELEPHANT) facility at Dartmouth College was designed to understand the interaction of plasma thermal particle detectors with ionospheric-like plasma<sup>1</sup>. In an experiment, an argon plasma is injected in a cylindrical vacuum chamber from a plate located at one end, through 21 bore holes, each one of radius 1.9 mm. After being injected, the plasma expands radially to form a beam which then extends over the full length of the vacuum chamber. The vessel contains a conducting sphere located near the cylinder axis, approximately 50 cm from the plasma injection region, as illustrated in Figs. 1 and 2. In addition, as shown in the figures, two movable cylindrical Langmuir probes mounted on a spin table are used to measure current voltage (I-V) characteristics at different locations near the sphere. The goal of the experiment is to study plasma properties in the vicinity of an immersed conducting body and thus develop a better understanding of the physics relevant to satellite-plasma interaction under well controlled laboratory conditions. More details about the experimental setup and plasma injection can be found in articles by Frederick-Frost and Lynch<sup>1</sup>, Gayetsky and Lynch<sup>3</sup>, and Fisher, et al.<sup>4</sup>. In the experiment, the plasma density, electron temperature and plasma potential were inferred from interpreting probe measurements using Langmuir probe theory<sup>5</sup>.

ELEPHANT is one of several experiments made over the years to study supersonic plasma flow around a conducting body. Perturbations caused by spacecraft in surrounding plasma are of interest because of their impact on particle sensors. For LEO satellites orbiting at supersonic speeds, these perturbations are particularly important in the wake of a satellite, which is

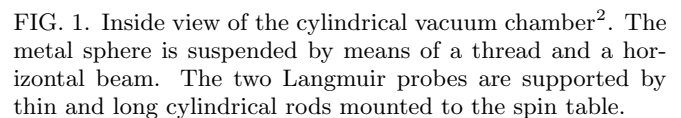


FIG. 1. Inside view of the cylindrical vacuum chamber<sup>2</sup>. The metal sphere is suspended by means of a thread and a horizontal beam. The two Langmuir probes are supported by thin and long cylindrical rods mounted to the spin table.

almost totally depleted of ions and neutral particles. Due to their large thermal speed (larger than the satellite speed) however, electrons can penetrate the wake leading to a negative space charge density and a relative negative potential in that region. This in turn affects the collection of background plasma particles, since practically no neutrals or ions can be collected, and only electrons with energies sufficient to overcome the potential barrier created by the wake negative charge density, can be collected. Moreover, when an electron probe is located in the wake, it collects electrons which, in general, are decelerated and deflected by the wake electric field, as well as by any sheath electric field at the

<sup>a)</sup>saeed\_physics@yahoo.com

probe itself. The importance of these interactions led to several theoretical, laboratory, and *in situ* studies aimed at a better understanding the dynamics of supersonic plasma flow near a material obstacle. For example Jastrow and Pearse, considered the deflection of positive ions around a negatively charged satellite to show that the resulting drag on LEO satellites can be comparable to that associated with neutral particle impacts<sup>6</sup>. A review of ionospheric dynamics in the presence of supersonic objects with various idealized geometries was presented by Guerevich, et al.<sup>7</sup>. More recently, a number of computational studies of spacecraft environment interaction have been reported in the literature as, for example, by Miyake, et al.<sup>8</sup>, Rehman, et al.<sup>9</sup>, and Davis, et al.<sup>10</sup>. On a related topic several authors have constructed models and provided analytic or tables of computed Langmuir probes characteristics under a variety of conditions, including low density collisionless plasmas<sup>11</sup>, magnetized<sup>12,13</sup>, magnetized plasmas with drift<sup>14</sup>, and plasmas drifting at supersonic flows<sup>15</sup>, to name a few. Laboratory experiments conducted under well controlled and diagnosed conditions have also been made to benchmark theoretical and model predictions. For example an early study by Clayden<sup>16</sup>, Stone<sup>17,18</sup>, Enloe, et al.<sup>19</sup>, and Meassick and Chan<sup>20</sup>. An interesting case of simulating a laboratory argon plasma by using SPIS code has been studied<sup>21</sup>. In this study, simulation results were compared with measured IV sweeps and the orbital and radial motion models. It was determined that radial motion models provide a better estimation of the slow ion density, which are produced by charge exchange reaction in the plasma tank. Finally observations have been made *in situ*, in order to understand spacecraft environment interaction under actual space plasma conditions. Without attempting an exhaustive literature review we mention, for example, experiments made with the Ariel I satellite by Samir and Willmore<sup>22</sup>, on orbit experiments with the Gemini/Agema two-body system by Troy, et al.<sup>23,24</sup>, on-board the space shuttle by Raitt, et al.<sup>25,26</sup>, Murphy, et al.<sup>27</sup>, and Enloe, et al.<sup>28</sup>.

The goal of this paper is to propose a protocol for validating simulation results of supersonic plasma flow diagnosed with two or more Langmuir probes. Validation is provided by the consistency between characteristics measured by the different probes at different locations, and simulated characteristics, for a unique set of upstream plasma parameters. Given these upstream conditions, it is suggested that kinetic simulation results can then be used to infer plasma parameters in a larger region between and around the probes. In order to achieve this goal, simulations must be carried out under conditions which are as realistic as possible, accounting in particular, for the detailed 3D system geometry, sheath electric fields, density and temperature gradients, and possibly magnetic field effects. This in turn should provide a more reliable means of interpretation of Langmuir probe measurements, which is independent of commonly made as-

sumptions such as a spatially uniform Maxwellian background plasma.

In the following, we use the particle in cell code PTetra<sup>29</sup> to calculate the characteristics of two probes in a selected ELEPHANT experiment. A full description of our model is contained in the cited reference. The validity of PTetra has been ascertained for different plasma conditions by reproducing known results obtained analytically<sup>30</sup> or numerically using other approaches<sup>15,31,32</sup>. PTetra results can generally be made to agree with established results within approximately 1% or less. In summary, PTetra is an explicit electrostatic PIC code in which the simulation domain is represented with an unstructured adaptive tetrahedral mesh. The main advantage of such a mesh is that it can be used to account for realistic experimental geometries. In the ELEPHANT experiment considered here, one probe is located upstream of a conducting sphere, while the other is downstream in the wake region. In these simulations, only the electron density  $n_e$  and temperature  $T_e$  in the injection region of the vacuum chamber are used as adjustable parameters. By fitting measured and computed characteristics at the two probe locations using only these two parameters in the injection region, the consistency of our simulations is established, thus supporting the validity of simulation results between the two probes and in their vicinity. Then by comparing simulated densities and temperatures at the probe positions, with those inferred experimentally with standard Langmuir probe theory, the importance of carrying out custom simulations is demonstrated.

Section II which follows, describes the specifics of the simulations. The comparison of simulated and measured I-V curves and plasma parameters are presented in Sec. III. In Sec. IIIB, we discuss the importance of accounting for Earth magnetic field in the experiment. Finally, in Sec. IV, we present a summary of our findings and some concluding remarks.

## II. NUMERICAL MODELING OF THE EXPERIMENT

The geometry of the experimental setup and simulation mesh are constructed using the open source mesh generator gmsh<sup>33</sup>. Our simulation domain accounts for the main features of the experimental setup, as illustrated in Fig. 2. It consists of a vacuum vessel, a sphere and two small cylindrical Langmuir probes. The probe closer to the source region is referred to as the upstream probe whereas the one in the wake region, as the downstream probe. The isolating probe supports, the spin table and the connecting wires are not included in the geometry for simplicity. The assumption made here is that owing to the orientation of the probe posts (perpendicular to the supersonic plasma flow) and the location of the spin table (well below the axis of the chamber where the plasma density is low), these structures should have a negligible effect on plasma at the probe locations.

TABLE II. Measured and fitted plasma parameters<sup>2</sup>. Unless stated otherwise, all simulation results are obtained with the magnetic field given in the table.

Plasma drift velocity	$\vec{v}_d \simeq 7500\hat{z}$ m/s
Ion temperature	$T_i \simeq 0.3$ eV
Neutral density	$n_n \simeq 8 \times 10^{17}$ m <sup>-3</sup>
Plasma density	$n_p \simeq 1 \times 10^{11}$ m <sup>-3</sup>
Local magnetic field	$\vec{B} = (-11.45, -31.82, -6.02)\mu\text{T}$
Electron density	$n_e$ =Fitted
Electron temperature	$T_e$ =Fitted
Plasma potential	$V_p$ =Fitted

FIG. 2. Geometry representing the experimental structures constructed with gmsh<sup>2</sup>. In this system of coordinate,  $X$  is out of the page.

The dimensions of the vacuum vessel and the relative positions and sizes of the sphere and Langmuir probe tips are shown in Fig. 2 and given in Table I. The parameters

TABLE I. Dimensions of the physical structures accounted for in the simulations<sup>2</sup>. The positions of the central sphere, and of the two probes are also given in the table.

Langmuir probe radius	0.16 cm
Langmuir probe length	1 cm
Sphere radius	5.08 cm
Plasma injection disc radius	18.4 cm
Chamber radius	61 cm
Chamber ends radius of curvature	106 cm
Chamber length	152 cm
Coordinates of the center of sphere	(0, 5.87, 40.64) cm
Coordinates of the upstream probe	(0.35, 5.87, 27.33) cm
Coordinates of the downstream probe	(0.35, 5.87, 48.18) cm

of the injected plasma, including the local (Earth) magnetic field and neutral density are given in Table II. Neutral particles are neglected in the simulations due to the estimated relatively large ion collisional mean free path  $> 1$  m with neutrals, although we recognize that charge-exchange ion populations may be significant in this experiment. In this table, variables identified with ‘‘Fitted’’ are those that had to be determined experimentally from probe measurements. The first step in our simulations is to determine the values of  $n_e$  and  $T_e$  in the injection region. This is done by computing the characteristic of the upstream probe and selecting the electron density and temperature in the injection region which best fit the

measured characteristic. This is obtained by minimizing the mean square difference between the computed  $I_c(V)$  and measured  $I_m(V)$  currents as

$$D(n_e, T_e) = \frac{1}{N} \sum_{i=1}^N |I_c(V_i) - I_m(V_i)|^2. \quad (1)$$

In practice,  $D$  is minimized by a) computing  $D$  on a rectangular grid in the  $n_e$   $T_e$  plane, b) identifying a point near the minimum, c) computing  $D$  on a finer grid near that point and d) estimating the minimizing values of  $n_e$  and  $T_e$  from a parabolic fit. The resulting values of  $n_e$  and  $T_e$  are then used to compute the upstream probe characteristic, and compare it to measurements. The consistency of our model is verified by using the same values of  $n_e$  and  $T_e$  in simulations to compute the downstream (in the wake) probe characteristic and compared it with the measurements. In the computer model, an argon plasma is injected from the whole disc surface as well as the contiguous lateral surface rather than from the 21 bore holes in the injection disc as in the experiment. The actual plasma injection through the 21 bore holes would be very difficult to simulate because a much higher plasma density would have to be modeled in each hole, characterized by significantly larger plasma frequency and smaller Debye length than in the vacuum chamber. As a result, a very fine mesh, sufficient to resolve each hole as well as the Debye length, would be needed in the injection region. Finally, PTetra being explicit, and the fact that most particles should not cross more than one cell in one time step, very small time steps would be required. The sphere and the probes considered here are at a distance of  $\sim 50$  cm from the 21 bore holes of the plasma injector. It is assumed that this distance is sufficiently large for the particle distributions at the positions of interest to be relatively independent of the exact distribution at the injector. A drifting Maxwellian distribution is then assumed for simplicity, for both electron and ion species at the injection surfaces.

### III. I-V CHARACTERISTICS

In the computation of the I-V characteristics, both upstream and downstream probes are biased simultaneously at discrete voltages with respect to the ground (the vacuum vessel). This is different from the experiment, in which characteristics are measured for only one probe at a time. That is, when a probe is biased to different voltages, the other one is left floating. By biasing both probes to the same potential in the simulations, it is possible to obtain the characteristics for both probes with half the simulation time of what would be required if each probe were biased separately. This procedure, however, is valid only if one probe's bias voltage has negligible influence on the other probe's characteristic, that is, if there is no 'crosstalk' between the probes. In order to assess crosstalk at locations shown in Fig. 2, two cases were simulated. In the first case, the upstream probe was biased to the highest voltage of +10 V, while the downstream probe was left floating. In the second case, the downstream probe was biased to +10 V, while the upstream probe was left floating. Compared to the simulations made with simultaneous biasing, case 1 showed no significant difference, and case 2 led to an increase in the collected current by the downstream probe by approximately 5%. It is therefore concluded that crosstalk is negligible, and that the simplification consisting of biasing both probes simultaneously to the same voltage leads to characteristics that are within 5% or less of the actual biasing procedure in which only one probe is biased at a time.

#### A. Optimization of $n_e$ and $T_e$ in the injection region

Applying this approach to a selected experiment, the optimized parameters are calculated to be  $n_e = 1.25 \times 10^{11} \text{ m}^{-3}$  and  $T_e = 0.647 \text{ eV}$  in the plasma injection region. A comparison between measured and computed (using these optimized parameters) characteristics is given in Fig. 3. In PTetra these adjustable parameters are specified at the plasma injection region only, and the plasma density and temperature are determined self-consistently in the remainder of the vacuum chamber. The good agreement between computed and measured characteristics in the wake region, using parameters optimized to fit characteristics upstream of the sphere, provides evidence of the consistency of our kinetic simulations. Using the above fitted parameters at the injection site, a case is simulated without the probes to determine the unknown plasma potential, electron density and temperature at the probe locations. Cross sections of these parameter profiles in the plane passing through the center of the sphere are shown in Fig. 4. In all three cases, significant spatial variations are found in the region of interest. This is to be contrasted with uniform profiles generally assumed in the interpretation of probe measurements us-

ing theoretical or computational models. A comparison of the electron density, temperature and the plasma potential, inferred experimentally, with the corresponding computed values determined from Fig. 4, is presented in Table III for both upstream and downstream probes. Experimentally the electron density, temperature and the

TABLE III. Comparison between the measured and computed electron density ( $n_e$ ), temperature ( $T_e$ ) and plasma potential ( $V_p$ ) relative to the vacuum chamber at the upstream probe (Up) and downstream probe (Dp) positions.

Parameters	Measured		Computed	
	Up	Dp	Up	Dp
$n_e \text{ (m}^{-3}\text{)}$	$3.17 \times 10^{11}$	$9.58 \times 10^{10}$	$0.98 \times 10^{11}$	$1.28 \times 10^{10}$
$T_e \text{ (eV)}$	0.45	0.54	0.64	0.47
$V_p \text{ (V)}$	2.45	1.71	2.61	1.30

plasma potential were determined by fitting electron currents (measured current from which the ion current was subtracted) with equation<sup>34</sup>

$$I_e = en_e A \left( \frac{kT_e}{2\pi m_e} \right)^{1/2} \exp \left( \frac{eV}{kT_e} \right), \quad (2)$$

where  $A$  is the effective probe area, and the probe potential  $V$  is assumed to be close to the plasma potential. We recall that this expression is based on a number of assumptions, including a collisionless electrons

FIG. 4. Cross sections of the electron density (a), temperature (b) and plasma potential (c) profiles in the  $X - Z$  plane passing through the center of the sphere. These profiles are obtained from a PTetra simulation using the electron density and temperature which best fit the characteristic measured by the upstream probe.

described by a Maxwellian distribution function, and a Debye length much smaller than the linear scale of the probe. In the present study, the Debye length (1.9) cm is approximately 12 times greater than the probe radius (0.16) cm, for which the above assumption is not satisfied. The comparison shows good agreement for the electron temperature and plasma potential but the simulated and experimentally measured densities are seen to be significantly different. In particular, the temperature and plasma potential at the location of the upstream and downstream probes agree within 30%. The ratios between measured and simulated densities, on the other hand, are of order 3.3 for the upstream probe and  $\sim 7.5$  for the downstream probe. This larger difference found for the downstream probe is consistent with the fact that the wake is a strong gradient region under the influence of the sphere electric sheath, and particle distributions there are likely farther from a Maxwellian. Under these conditions the interpretation of measured characteristics based on standard Langmuir probe theories, in which homogeneous and Maxwellian plasmas are assumed, is likely not applicable.

## B. Magnetic field effects

One of the motivations of this work is to demonstrate the importance of kinetic and nonlocal effects when interpreting particle sensor measurements in plasma with strong gradients, or when measurements are made close to material objects. Variations in density, temperature, and potential, occurring on a scale length of order of

one to a few centimeters are clearly visible in Fig. 4. These variations, combined with electrons magnetization in Earth magnetic field in the lab, can lead to significant deviations from a Maxwellian distribution function in this experiment. With the magnetic field given in Table II and the electron temperature in the injection region, the electron thermal gyro-radius is estimated to be  $\rho_{th,e} = \sqrt{2T_e/m_e} \times m_e/(eB) \sim 7$  cm, where  $m_e$  is the electron mass. This is comparable to scale lengths characterizing variations in plasma profiles in the chamber, and it therefore enhances the non locality of measurements made at probe locations. The effect of Earth magnetic field and resulting electron magnetization is shown in Fig. 5, where cross sections of the electron velocity distribution functions are shown as calculated without and with magnetic field taken into account. The velocity distributions shown in this figure were calculated at point  $P$  shown in Fig. 2 close to the plasma injector, using test-kinetic particle back-tracking and electric fields obtained with PTetra simulations<sup>35-38</sup>. In this experiment, only electrons are magnetized. Due to their large mass and gyro-radius, argon ions are not affected by the local magnetic field, and their distributions are not shown here. In

FIG. 5. Electron velocity distribution functions 5 cm from the source region with (panels b and d) and without (panels a and c) magnetic field in a  $V_x - V_y$  plane (top panels) and a  $V_z - V_x$  plane (bottom panels)<sup>2</sup>. The velocities along the axes are normalized to the electron thermal velocity,  $v_{th} = \sqrt{T_e/m_e}$ .

the absence of a magnetic field, the electron distribution is a Maxwellian in the  $V_x - V_y$  plane and it is a truncated Maxwellian in  $V_z - V_x$  plane. The truncation here is due to the fact that the electrons are drifting in the positive  $z$  direction and do not return back to the source region. This is why the distribution function vanishes there for  $V_z < 0$ . As shown in panel b and d of Fig. 5, the local

magnetic field leads to complex structures in the electron distribution function. This complexity arises due to the Lorentz force experienced by the electrons. These filamentary structures are due to the electron thermal gyro-radius  $\sim 7$  cm, being comparable to the linear dimension of the injection region, and the fact that the point being considered is not sufficiently far from the end of the injection chamber (5 cm from the end) for injected electrons to have isotropized. The structures in these distributions are further verified by plotting sample electron trajectories reaching point  $P$  and originating from the injection surfaces. Figure 6 shows the trajectories of 100 electrons which are integrated backward in time from the point where these distribution functions are computed with  $\vec{B}$  (red) and without  $\vec{B}$  (green). This shows that the gy-

FIG. 6. Electron trajectories computed with (red) and without (green) the local magnetic field. The trajectories are calculated using backtracking from the point  $P$  shown in Fig. 2. Numbers along the axes are in chamber coordinates; the entire  $x$  axis length corresponds to the diameter of the plasma injection disc.

ration along the field lines causes some electrons to turn around and propagate in the  $-z$  direction at the point considered, thus leading to a non zero distribution function when  $V_z < 0$  in panel d, and beak-like structure in the distribution in panel b.

The effect of Earth magnetic field on macroscopic profiles is also visible in Fig. 7, in which cross sections of the electric potential are shown in the  $Y = 0$  plane, when computed without and with Earth magnetic field. The effect here is more subtle than with the electron particle distributions, but the two panels of the figure show clear differences in the profiles. In particular without a magnetic field, the lateral regions above and below the sphere are seen to be “enveloped” by a higher potential layer, and the potential in the wake is also noticeably larger when  $B = 0$  than when  $B \neq 0$ . The figure also shows that the potential difference between the wake region on axis, and plasma off axis, are larger when  $B = 0$ , thus

FIG. 7. Cross sections of the plasma potential profiles in the  $X - Z$  plane passing through the center of the sphere computed without (a) and with (b) Earth magnetic field. These profiles are obtained from a PTetra simulation using the electron density and temperature which best fit the characteristic measured by the upstream probe.

resulting in larger radial electric fields in that region.

The effect of Earth magnetic field on the probe characteristics is found to be relatively weak, as shown in Fig. 3. This is in contrast with noticeable differences in the profiles of the electric potential seen in Fig. 7, and the significant differences in the electron distribution functions and trajectories shown in Figs. 5 and 6. In view of these differences, we therefore believe that the Earth magnetic field should be accounted for in similar simulations even if its effect on the two probes considered in this particular experiment are relatively unimportant.

#### IV. SUMMARY AND CONCLUSIONS

A laboratory plasma experiment is simulated with the PIC code PTetra, and the consistency of our computational approach is established by comparing simulated and experimental characteristics. The experiment conducted under well controlled and diagnosed conditions, was designed to study basic physics relevant to satellite interaction with space environment. In the experiment, an argon plasma interaction with a metallic spherical body in a vacuum chamber is studied. The current voltage (I-V) characteristics of cylindrical Langmuir probes are measured upstream and downstream of a grounded conducting sphere, from which plasma parameters are inferred using standard Langmuir probe theory. In the simulations, the electron density and

temperature at the injection region of the chamber are adjusted in order to best fit measured characteristics at the upstream probe location. Then using the same parameters, the computed characteristic of the downstream probe is shown to be in good agreement with the one obtained experimentally. Plasma parameters inside the chamber are computed and compared with measured values at the probe locations. The electron temperature and plasma potential in the chamber are found to be well reproduced while computed electron densities are appreciably lower than the ones inferred from local probe theory. Furthermore, the electron thermal gyro-radius is found to be comparable to scale lengths characterizing plasma parameter profiles in the vacuum vessel, and to the distance between probes and the conducting sphere. Electron magnetization is also shown to produce significant deviations from a Maxwellian velocity distribution, even close ( $\sim 5$  cm) to the injection region, where plasma is injected as per a drifting Maxwellian distribution. Combined with spatial gradients in the plasma density and temperature near the probe locations, the finite electron magnetization further accentuates the nonlocal response of the probes to nearby plasma. That is, characteristics are not determined by local plasma parameters at probe locations, but rather by a convolution of these parameters near the probes.

In conclusion, the consistency between the characteristics measured and simulated, for probes at different locations found in this experiment, supports the idea of extending this approach to improve the interpretation of Langmuir probe measurements in supersonic plasma flows. With results from detailed kinetic simulations accounting for the system geometry, a background magnetic field, and other important physical effects, it is suggested that such simulations could be used to determine the spatial distribution of plasma macroscopic and microscopic properties not only at probe locations themselves, but over a broader region between and surrounding them. This last suggestion cannot be fully verified here owing to the presence of only two probes in the experiment. Further studies aimed at assessing the validity of the proposed methodology should be conducted in laboratory or space plasma, with three probes or more. It would then be possible to ascertain to what extent and over which regions of space, consistency between measured and simulated characteristics using a subset of probes optimally located, can lead to similar consistency between measured and simulated characteristics at other locations.

## ACKNOWLEDGMENTS

This work was supported in part by the Natural Sciences and Engineering Research Council of Canada. Work for the MICA mission at Dartmouth was supported by NASA Grant No. NNX10AL18G, NASA space

Grant No. NNX10AL97H, and by Dartmouth Colleges Presidential Scholar and Senior Honors Thesis programs. Simulation results presented in this article were obtained with the Westgrid computational infrastructure.

- <sup>1</sup>K. M. Frederick-Frost and K. Lynch, Rev. Sci. Instrum. **78**, 075113 (9 pp.) (2007).
- <sup>2</sup>S. ur Rehman, *Simulation of Space Environment Effects On Particle Sensors*, Ph.D. thesis, Department of Physics, University of Alberta, Canada (2014).
- <sup>3</sup>L. Gayetsky and K. Lynch, Rev. Sci. Instrum. **82**, 046112 (3 pp.) (2011).
- <sup>4</sup>L. Fisher, K. Lynch, P. Fernandes, T. Bekkeng, J. Moen, M. Zettergren, R. Miceli, S. Powell, M. Lessard, and P. Horak, Review of Scientific Instruments **87**, 043504 (2016).
- <sup>5</sup>H. Mott-Smith and I. Langmuir, Physical Review **28**, 727 (1926).
- <sup>6</sup>R. Jastrow and C. Pearce, Journal of Geophysical Research **62**, 413 (1957).
- <sup>7</sup>A. V. Gurevich, L. Pitaevskii, and V. Smirnova, Space Science Reviews **9**, 805 (1969).
- <sup>8</sup>Y. Miyake, C. Cully, H. Usui, and H. Nakashima, Journal of Geophysical Research: Space Physics **118**, 5681 (2013).
- <sup>9</sup>S. U. Rehman, R. Marchand, J.-J. Berthelier, T. Onishi, and J. Burchill, IEEE Trans. Plasma Sci. **41**, 3402 (2013).
- <sup>10</sup>V. Davis, M. Mandell, D. Cooke, and C. Enloe, Journal of Geophysical Research: Space Physics **104**, 12445 (1999).
- <sup>11</sup>J. G. Laframboise, *Theory of spherical and cylindrical Langmuir probes in a collisionless, Maxwellian plasma at rest*, Ph.D. thesis, University of Toronto (1966).
- <sup>12</sup>J. R. Sanmartin, Phys. Fluids **13**, 103 (1970).
- <sup>13</sup>J. Laframboise and L. Sonmor, Journal of Geophysical Research **98**, 337 (1993/01/01).
- <sup>14</sup>J. Rubinstein and J. Laframboise, Phys. Fluids **26**, 3624 (1983).
- <sup>15</sup>L. Patacchini and I. Hutchinson, Plasma Phys. Control. Fusion **53**, 025005 (23 pp.) (2011).
- <sup>16</sup>W. Clayden, in *Rarefied Gas Dynamics, Volume 2*, Vol. 1 (1963) p. 435.
- <sup>17</sup>N. H. Stone, J. Plasma Phys **25**, 19816 (1981).
- <sup>18</sup>N. H. Stone, Journal of Plasma Physics **26**, 385 (1981).
- <sup>19</sup>C. Enloe, D. Cooke, S. Meassick, C. Chan, and M. Tautz, Journal of Geophysical Research: Space Physics **98**, 13635 (1993).
- <sup>20</sup>S. Meassick and C. Chan, Journal of Geophysical Research **99**, 19597 (1994/10/01).
- <sup>21</sup>J. C. Mateo-Velez, J. F. Roussel, D. Sarrail, F. Boulay, V. Inguibert, and D. Payan, IEEE Transactions on Plasma Science **36**, 2369 (2008).
- <sup>22</sup>U. Samir and A. Willmore, Planetary and Space Science **13**, 285 (1965).
- <sup>23</sup>B. E. Troy Jr, D. B. Medved, and U. Samir, Journal of the Astronautical Sciences **18**, 173 (1970).
- <sup>24</sup>B. E. Troy, E. Maier, and U. Samir, Journal of Geophysical Research **80**, 993 (1975).
- <sup>25</sup>W. Raitt, D. Siskind, P. Banks, and P. Williamson, Planetary and space science **32**, 457 (1984).
- <sup>26</sup>W. Raitt, J. Eccles, D. Thompson, P. Banks, P. Williamson, and R. Bush, Geophysical research letters **14**, 359 (1987).
- <sup>27</sup>G. Murphy, D. Reasoner, A. Tribble, N. D'Angelo, J. Pickett, and W. Kurth, Journal of Geophysical Research: Space Physics **94**, 6866 (1989).
- <sup>28</sup>C. Enloe, D. Cooke, W. Pakula, M. Violet, D. Hardy, C. Chaplin, R. Kirkwood, M. Tautz, N. Bonito, C. Roth, G. Courtney, V. Davis, M. Mandell, D. Hastings, G. Shaw, G. Giffin, and R. Segal, Journal of Geophysical Research **102**, 425 (1997/01/01).
- <sup>29</sup>R. Marchand, IEEE Trans. Plasma Sci. **40**, 217 (2012).
- <sup>30</sup>J. G. Laframboise, *Theory of Spherical and Cylindrical Langmuir Probes in a Collisionless, Maxwellian Plasma at Rest.*, Ph.D. thesis, UNIVERSITY OF TORONTO (CANADA). (1966).
- <sup>31</sup>L. Patacchini, I. H. Hutchinson, and G. Lapenta, Phys. Plasmas **14**, 062111 (8 pp.) (2007).

<sup>31</sup>L. Patachini and I. Hutchinson, Plasma Phys. Control. Fusion **52**, 035005 (19 pp.) (2010).

<sup>33</sup>J. Guenneau and J.-F. Remacle, Int. J. Numer. Meth. Eng. **79**, 1309 (2009).

<sup>34</sup>F. F. Chen, IEEE-ICOPS meeting, Jeju, Korea (June 2003).

<sup>35</sup>T. Speiser, J. Geophys. Res. **70**, 1717 (1965).

<sup>36</sup>R. Richard, R. Walker, and M. Ashour-Abdalla, Geophys. Res. Lett. **21**, 2455 (1994).

<sup>37</sup>R. Marchand, J. L. F. Mackay, and K. Kabin, Plasma Phys. Cont. Fusion **50**, 074007 1 (2008).

<sup>38</sup>R. Marchand, Commun. Comput. Phys. **8**, 471 (2010).

ACCEPTED MANUSCRIPT



Bore hole

Sphere

Spin table  
assembly

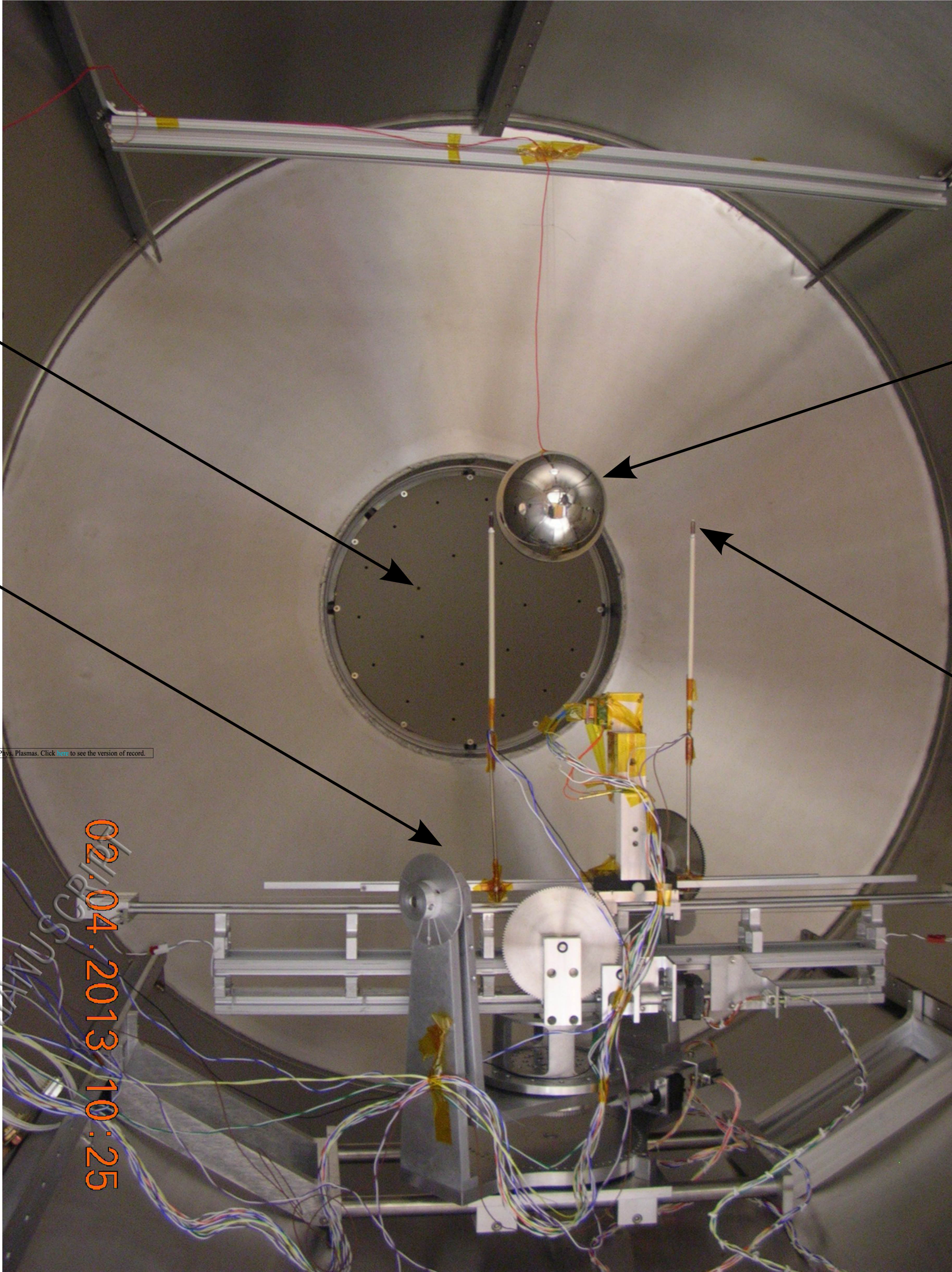
Langmuir probe

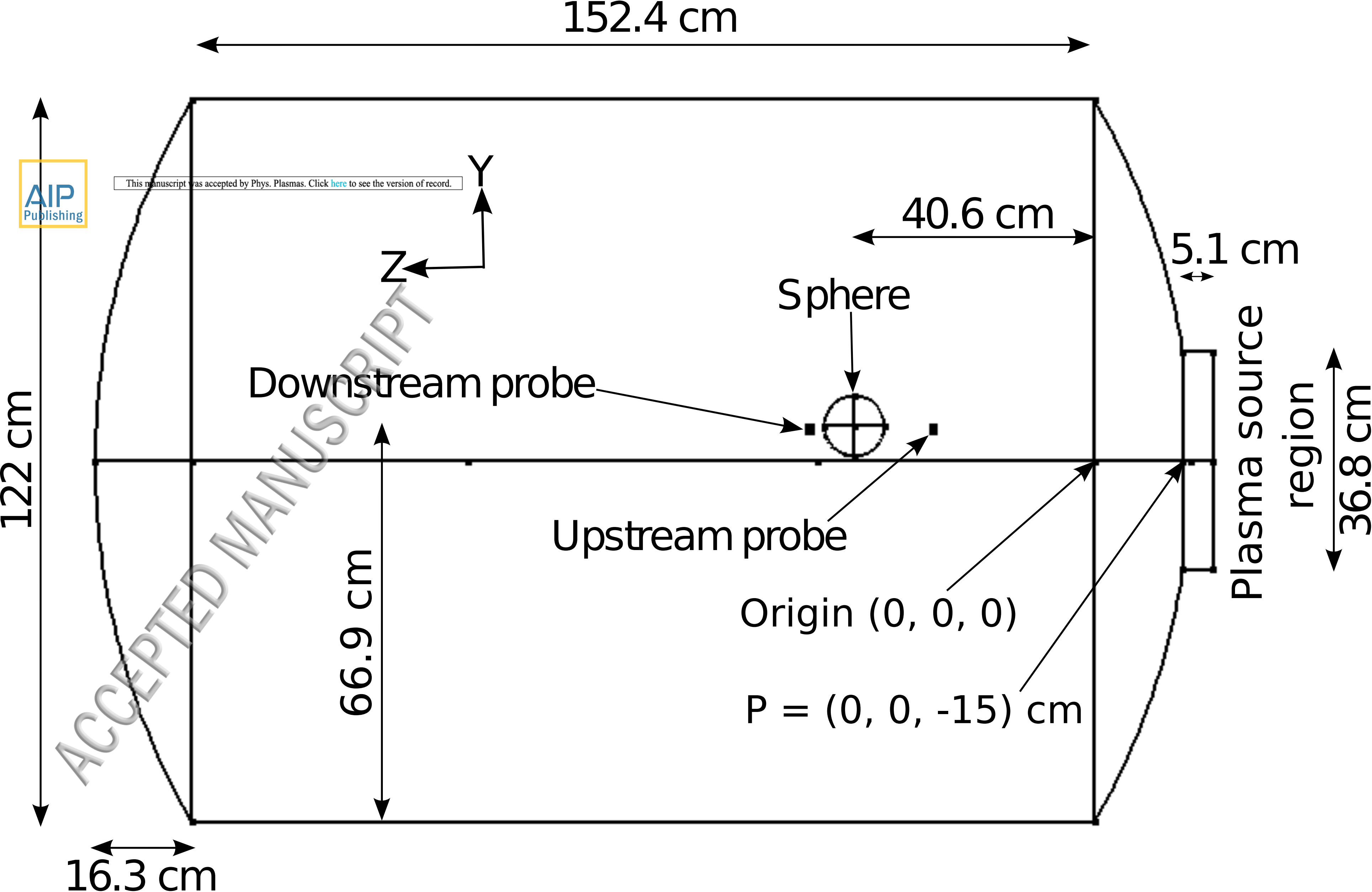


This manuscript was accepted by Phys. Plasmas. Click [here](#) to see the version of record.

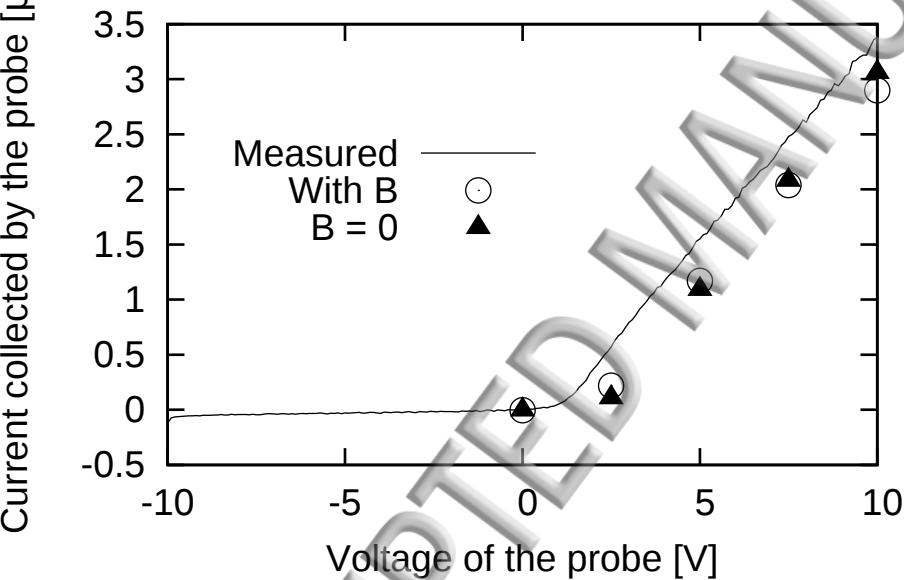
02.04.2013 10:25

ACCEPTED MANUSCRIPT





## Upstream Langmuir probe characteristics



## Downstream Langmuir probe characteristics

